Chapter 7
Global Buckling of Sandwich Columns and Wide Panels

The most important issue regarding buckling of sandwich structures is the effect of transverse shear which can significantly reduce the Euler critical load. Simply put, the effect of transverse shear absolutely cannot be neglected. Therefore, all formulas for sandwich buckling are essentially ways to include this effect into the Euler formulas. Two basic ways for including transverse shear in column buckling are the Engesser (1891) and the Haringx (1948, 1949) approaches. Both of these approaches are also outlined by Timoshenko (1936).

In this chapter, some of the most widely used column buckling approaches will be presented and compared, followed by the application of first-order shear analysis to the buckling of wide panels and simply supported rectangular panels. Panel compression test methods and data reduction analysis for the evaluation of the critical load will be presented along with examples and collapse strength estimates.

7.1 The Engesser Approach

The Engesser approach is based on considering the additional slope and hence the additional curvature produced by the shear force. Consider the fixed-free sandwich column shown in Figure 7.1a, which is loaded axially by a compressive load P . When buckling occurs, there will be shear forces acting on the cross-sections of the column (Figure 7.1b). The magnitude of the shear force Q acting at a cross-section mm can be found from Figure 7.1c:

$$Q \simeq P\frac{dw}{dx}. \tag{7.1}$$

L.A. Carlsson and G.A. Kardomateas, *Structural and Failure Mechanics of Sandwich Composites*, Solid Mechanics and its Applications 121, DOI 10.1007/978-1-4020-3225-7_7,

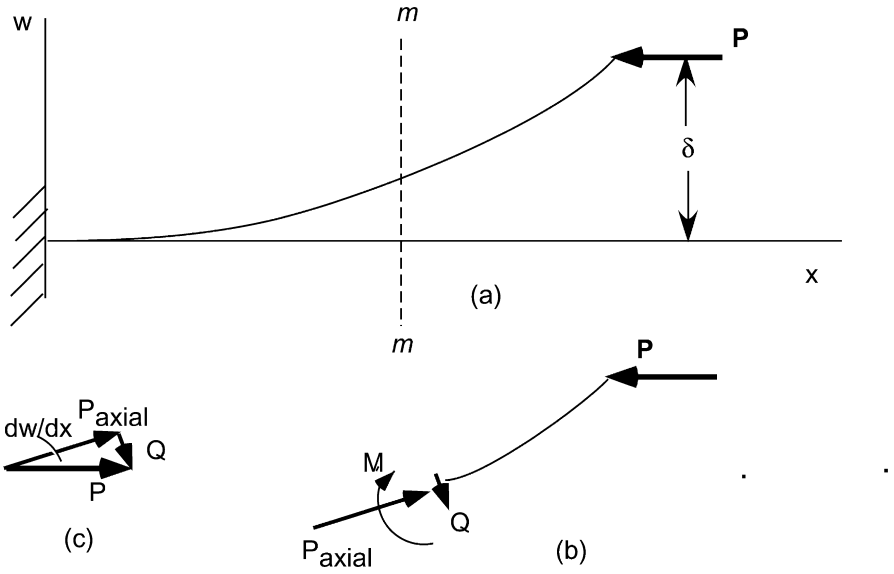

Figure 7.1 Forces and moments acting on a buckled sandwich column.

Note that at the section *mm* there will also be an axial force, $P_{\text{axial}} \simeq P$.

The change in slope of the deflection curve produced by the shear force is

$$\frac{\beta Q}{AG_{\text{eq}}}, \tag{7.2}$$

where A is the total cross-sectional area of the column, G_{eq} is the "equivalent" or "effective" modulus in shear, and β is a correction factor depending on the shape of the cross-section, which accounts for the fact that shear is not distributed uniformly throughout the section. If the section is rectangular and the column homogeneous isotropic, then $G_{\text{eq}} = G =$ shear modulus of the homogeneous material and $\beta = 1.2$. We shall discuss both G_{eq} and β for sandwich construction later in this section.

The rate of change of slope produced by the shear force Q represents the additional curvature due to shear and, from Equation (7.1), this is equal to

$$\frac{\beta}{AG_{\text{eq}}}\frac{dQ}{dx} = \frac{\beta P}{AG_{\text{eq}}}\frac{d^2w}{dx^2}.$$

The total curvature of the deflection curve is now obtained by adding the curvature produced by the shear force to the curvature produced by the bending moment. Thus, for the column of Figure 7.1a, the differential equation for the deflection curve becomes:

$$\frac{d^2w}{dx^2} = \frac{M}{(EI)_{\text{eq}}} + \frac{\beta}{AG_{\text{eq}}}\frac{dQ}{dx}\,, \tag{7.3a}$$

or

$$\frac{d^2w}{dx^2} = \frac{P(\delta - w)}{(EI)_{\text{eq}}} + \frac{\beta P}{AG_{\text{eq}}}\frac{d^2w}{dx^2}\,, \tag{7.3b}$$

where $(EI)_{\text{eq}}$ is the "equivalent" or "effective" bending rigidity of the sandwich cross-section (see Chapter 4 and discussion later).

Equation (7.3b) can be written as

$$\frac{d^2w}{dx^2} = \frac{P}{(EI)_{\text{eq}}[1 - \beta P/(AG_{\text{eq}})]}(\delta - w)\,. \tag{7.4}$$

If we set

$$k^2 = \frac{P}{(EI)_{\text{eq}}[1 - \beta P/(AG_{\text{eq}})]}, \tag{7.5a}$$

we can write (7.4) in the form

$$\frac{d^2w}{dx^2} + k^2 w = k^2\delta. \tag{7.5b}$$

The general solution of this equation is

$$w = A_1 \cos kx + A_2 \sin kx + \delta\,, \tag{7.5c}$$

in which A_1 and A_2 are constants of integration. These constants are determined from the fixed end conditions:

$$w = \frac{dw}{dx} = 0 \quad \text{at } x = 0. \tag{7.5d}$$

These two conditions are fulfilled if

$$A_1 = -\delta, \quad A_2 = 0 \tag{7.5e}$$

and then

$$w = \delta(1 - \cos kx). \tag{7.5f}$$

The condition at the free end of the column requires that

$$w = \delta \quad \text{at } x = L, \tag{7.5g}$$

which is satisfied if

$$\delta \cos kL = 0. \tag{7.6}$$

For a non-zero δ, the smallest value of kl which satisfies Equation (7.6) is $kl = \pi/2$, which when combined with (7.5) gives

$$\frac{P}{(EI)_{\text{eq}}[1 - \beta P/(AG_{\text{eq}})]} = \frac{\pi^2}{4L^2} \,. \tag{7.7}$$

Solving for P gives the critical load:

$$P_{\text{cr}} = \frac{P_E}{1 + \beta P_E/(AG_{\text{eq}})}, \tag{7.8}$$

where $P_E = \pi^2 (EI)_{\text{eq}}/(4L^2)$ represents the Euler critical load for this case.

7.2 The Haringx Approach

In this approach, due to the shear strain, γ, there is an additional slope measured from the normal to the section to the tangent to the axis of the deflected column. This additional slope is added to the slope, θ, due to the bending moment, measured from the x axis to the normal to the cross-section. Thus the slope of the deflected curve is by use of Equation (7.2):

$$\frac{dw}{dx} = \theta + \gamma = \theta + \frac{\beta Q}{AG_{\text{eq}}}. \tag{7.9}$$

The axial force P has a component in the direction normal to the section equal to $P \cos\theta \simeq P$ and a component

$$Q = P \sin\theta \simeq P\theta. \tag{7.10}$$

Substituting in Equation (7.9), the slope becomes

$$\frac{dw}{dx} = \theta + \frac{\beta P \theta}{AG_{\text{eq}}} = \theta \left(1 + \frac{\beta P}{AG_{\text{eq}}}\right). \tag{7.11}$$

Observing that

$$\frac{d\theta}{dx} = \frac{M}{(EI)_{\text{eq}}} = \frac{P(\delta - w)}{(EI)_{\text{eq}}},$$

we obtain from Equation (7.11) the following expression for the curvature:

$$\frac{d^2 w}{dx^2} = \frac{P(\delta - w)}{(EI)_{\text{eq}}} \left(1 + \frac{\beta P}{AG_{\text{eq}}}\right). \tag{7.12}$$

The difference between Equation (7.12) and the previous equation (7.4) is due to the fact that in the derivation of Equation (7.4) the shear force is calculated from the total slope dw/dx of the deflection curve (see Equation (7.1)), whereas in the derivation of Equation (7.12), only the angle of rotation of the cross-section is used (see Equation (7.10)).

Solving the differential equation (7.12) in the same manner as before we find that the critical load is

$$P_{\text{cr}} = \frac{\sqrt{1 + 4\beta P_E/(AG_{\text{eq}})} - 1}{2\beta/(AG_{\text{eq}})} \,. \tag{7.13}$$

Now one important note regarding Haringx's formula: In a recent paper, Bazant and Beghini (2006) showed that the Engesser and Haringx-type theories are equivalent (i.e., one to follow from the other) provided that a proper transformation of the shear modulus of the core, G_c, is made. However, this transfomation implies that G_c of the soft core is a function of the axial stress in the stiff face sheets. This paradox was clarified by showing that the energetic variational analysis merely requires that the shear stiffness of the cross-section, characterized by G_c of the core, to be a function of the axial force in the face sheets. In other words, if the Haringx-type theory was used with a constant shear modulus, results as in Equation (7.13) would be obtained. However, if the shear modulus is updated as a function of the axial load, then the results are expected to agree with Engesser's formula.

Equations (7.8) and (7.13), the first (Engesser's) are the most widely used. The Haringx formula is expected to have accuracy issues if a constant shear modulus is used (this will be confirmed in Section 7.6). In fact, the global buckling formulas for sandwich columns in the literature provide ways of defining the G_{eq} and $(EI)_{\text{eq}}$ for use in the Engesser's formula (7.8). In the following, we outline the Allen (1969), the Bazant and Cedolin (1991), and the Huang and Kardomateas (2002) approaches for defining these quantities.

7.3 Allen's Formulas

7.3.1 Thin Faces

With regard to the cross-section in Figure 7.2, Allen's formula for thin faces assumes that the equivalent bending rigidity is due to the face sheets only and the face sheets are considered as two areas fb, where b is the width of

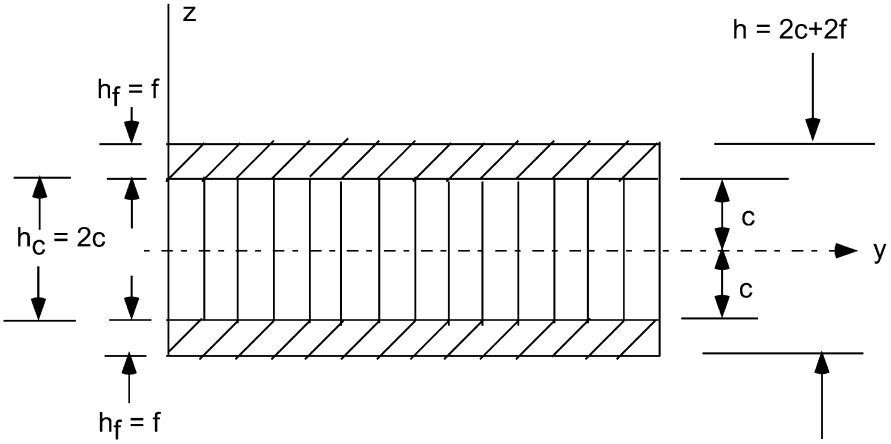

Figure 7.2 Sandwich cross-section.

the beam, located at a distance $c + f/2$ from the mid-axis (the neutral axis of the section), i.e.

$$(EI)_{\text{eq}} = 2E_f bf\left(c + \frac{f}{2}\right)^2. \tag{7.14a}$$

The equivalent shear modulus of the section is just the shear modulus of the core, and the shear correction factor in Equation (7.8) becomes

$$\frac{\beta}{AG_{\text{eq}}} = \frac{1}{b(2c+f)G_c}. \tag{7.14b}$$

Then, Equation (7.8) for a simply-supported column becomes

$$P_{\text{cr}} = \frac{P_E}{1 + P_E/(AG_c)}; \quad P_E = \frac{\pi^2}{L^2} 2E_f bf\left(c + \frac{f}{2}\right)^2. \tag{7.14c}$$

An alternative form of the above equation is

$$\frac{1}{P_{\text{cr}}} = \frac{1}{P_E} + \frac{1}{AG_c}, \quad A = b(2c+f). \tag{7.15}$$

This formula shows that when the sandwich construction involves a core of very low shear modulus, the critical load would be dominated by the second term of Equation (7.15), i.e. by the core, and it would approach the value AG_c. On the other hand, if the core shear modulus is very high, the critical load would be dominated by the first term of Equation (7.15), and it would approach the Euler load P_E.

7.3.2 Thick Faces

When the faces are thick, see Section 1.1, the bending rigidity of the faces about their own separate centroidal axes cannot be neglected. Therefore, the equivalent rigidity is now

$$(EI)_{\text{eq}} = E_f I = E_f(I_1 + I_f), \quad I_1 = 2bf\left(c + \frac{f}{2}\right)^2, \quad I_f = \frac{bf^3}{6}. \tag{7.16}$$

Note that again the bending rigidity of the core is neglected.

The Allen approach consists of considering that, at the buckled state, there occur two superimposed displacements, w_1 (the ordinary bending displacement) and w_2, an additional displacement associated with the shear deformation of the core.

The interaction between the bending stiffness of the faces and the shear stiffness of the core can be seen most easily if we first consider a sandwich with a core which is rigid in shear ($G_c = \infty$). A deflection w_1 occurs in accordance with ordinary bending theory. This deflection is associated with a bending moment M_1 and a shear force Q_1, the latter being

$$-Q_1 = (EI)_{\text{eq}}\frac{d^3w_1}{dx^3} = E_f I_1\frac{d^3w_1}{dx^3} + E_f I_f\frac{d^3w_1}{dx^3}. \tag{7.17}$$

The first term on the right-hand side of Equation (7.17) represents the shear force carried by the beam as a whole, supposing the faces to undergo only uniform extension or contraction without bending locally. In this state the shear stress τ is uniform across the thickness of the core and diminishes linearly to zero across the thickness of each face. The first term may therefore be replaced by $-b(2c + f)\tau$ where τ is the shear stress in the core:

$$-Q_1 = -b(2c + f)\tau + E_f I_f\frac{d^3w_1}{dx^3}. \tag{7.18}$$

As a result of the shear stress τ, the core undergoes a shear strain $\gamma_c = \tau/G_c$ which corresponds to an additional beam deflection w_2.

The shear deformation is illustrated in Figure 7.3, which shows a simply supported beam under three point bending. The points a, b, ... lie on the mid-lines of the faces and do not move horizontally (as in the ordinary bending w_1, case) but instead are displaced just vertically by w_2. The faces and the longitudinal center-line of the beam tilt, and the relationship between this additional slope of the beam dw_2/dx and the core shear strain can be obtained from Figure 7.4:

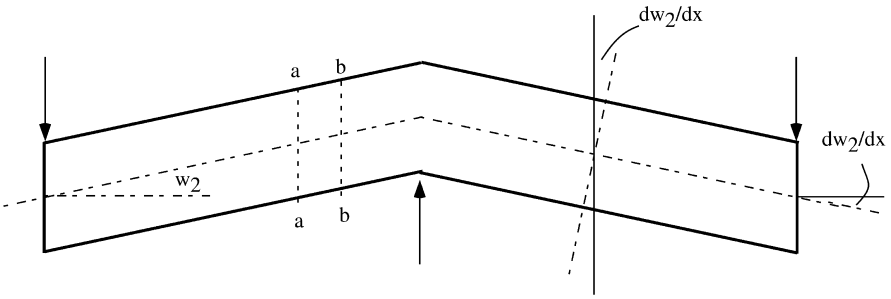

Figure 7.3 Additional beam deflection, w_2, due to transverse shear.

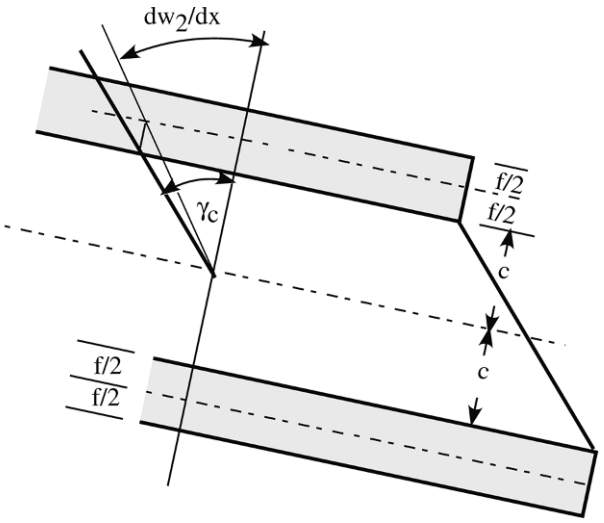

Figure 7.4 Schematic of the relationship between additional slope of the beam due to transverse shear and core shear strain.

$$c\gamma_c = \left(c + \frac{f}{2}\right)\frac{dw_2}{dx}, \tag{7.19a}$$

therefore

$$\tau = \left(1 + \frac{f}{2c}\right) G_c \frac{dw_2}{dx}. \tag{7.19b}$$

Substitution in Equation (7.18) yields

$$-Q_1 = -AG_c\frac{dw_2}{dx} + E_f I_f \frac{d^3 w_1}{dx^3}, \quad \text{where} \quad A = \frac{b(2c+f)^2}{2c}. \tag{7.20}$$

Rearranging the above equation and substituting $Q_1 = -(EI)_{\text{eq}} d^3 w_1/dx^3$ gives

$$\frac{dw_2}{dx} = -\frac{(EI)_{\text{eq}}}{AG_c}\left(1 - \frac{I_f}{I}\right)\frac{d^3w_1}{dx^3} = \frac{Q_1}{AG_c}\left(1 - \frac{I_f}{I}\right). \tag{7.21}$$

The additional transverse deflection w_2 corresponds to an additional shear force Q_2, since the faces must share this extra deflection and, in order to do so, they must be subjected to an additional bending moment and shear force, hence the total shear force is

$$Q = Q_1 + Q_2 = Q_1 - E_f I_f \frac{d^3w_2}{dx^3}.$$

Substitution of d^3w_2/dx^3 from (7.21) provides a differential equation for Q_1:

$$\frac{d^2Q_1}{dx^2} - \lambda^2 Q_1 = -\lambda^2 Q, \tag{7.22a}$$

where

$$\lambda^2 = \frac{AG_c}{E_f I_f (1 - I_f/I)}. \tag{7.22b}$$

Now the total shear force is (Equation (7.1))

$$Q = P\frac{dw}{dx} = P\left(\frac{dw_1}{dx} + \frac{dw_2}{dx}\right).$$

Using (7.21) for the slope dw_2/dx in terms of Q_1, we obtain the following differential equation for Q_1:

$$\frac{d^2Q_1}{dx^2} - \left(\lambda^2 - \frac{P}{E_f I_f}\right) Q_1 = -\lambda^2 P \frac{dw_1}{dx}. \tag{7.23}$$

Substituting $Q_1 = -(EI)_{\text{eq}} d^3w_1/dx^3$ gives a differential equation for w_1:

$$\frac{d^5w_1}{dx^5} - \left(\lambda^2 - \frac{P}{E_f I_f}\right)\frac{d^3w_1}{dx^3} = -\frac{\lambda^2 P}{(EI)_{\text{eq}}}\frac{dw_1}{dx}. \tag{7.24}$$

Consider the case of simply-supported ends; then the boundary conditions are $w_1 = d^2w_1/dx^2 = 0$ at $x = 0, L$. These conditions are fulfilled by a sinusoidal displacement:

$$w_1 = a_1 \sin\frac{\pi x}{L}.$$

Substitution into (7.24) gives the following:

$$\left[\frac{\pi^4}{L^4} + \left(\lambda^2 - \frac{P}{E_f I_f}\right)\frac{\pi^2}{L^2} - \frac{\lambda^2 P}{E_f I}\right] a_1 = 0,$$

from which we obtain the critical load:

$$P_{\text{cr}} = \frac{\frac{\pi^4}{L^4} + \frac{\lambda^2\pi^2}{L^2}}{\frac{\pi^2}{L^2 E_f I_f} + \frac{\lambda^2}{E_f I}}. \tag{7.25}$$

This can be expressed in a more general form by using the following definitions:

$$P_E = \frac{\pi^2 E_f I}{L^2}, \quad P_{Ef} = \frac{\pi^2 E_f I_f}{L^2}, \quad P_c = AG_c = \frac{b(2c+f)^2}{2c} G_c, \tag{7.26}$$

where P_E is the Euler load of the entire sandwich column, P_{Ef} is the Euler load of the two faces when they buckle as independent struts, and P_c may be described as the shear buckling load, which is essentially numerically equal to the shear stiffness AG_c. In terms of these quantities, the critical load from Equation (7.25) can be expressed in the general form

$$P_{\text{cr}} = P_E \left[\frac{1 + \frac{P_{Ef}}{P_c} - \frac{P_{Ef}^2}{P_c P_E}}{1 + \frac{P_E}{P_c} - \frac{P_{Ef}}{P_c}} \right]. \tag{7.27}$$

When the faces are very thin, $P_{Ef} \to 0$ and Equation (7.27) coincides with the thin face formula (7.15).

One additional note: Allen's thick face formula, (7.27), turns out to be the prediction from the high-order sandwich panel theory (HSAPT) discussed in Section 6.2 in the limit when the core modulus approaches infinity ($E_c \to \infty$) (Frostig, 2010, personal communication).

7.4 Bazant and Cedolin's Formula

In this formula, the shear correction is defined as follows. Keeping the same notation, the rotation dw_1/dx of the cross-section is defined by the longitudinal displacements of the face centroids, which differs slightly from the rotation of the core cross-section (Figure 7.4). Denoting by γ_c the shear strain in the core and by γ the average shear strain (which is dw_2/dx in the previous section), we can see from Figure 7.4:

$$\left(c + \frac{f}{2}\right)\gamma = c\gamma_c. \tag{7.28a}$$

This is the same as the relation (7.19a) derived in the previous section. Therefore,

$$\gamma_c = \frac{Q}{G_c(2cb)} = \left(1 + \frac{f}{2c}\right)\gamma. \tag{7.28b}$$

Solving for γ, which is the difference between the slope dw/dx of the deflected beam axis and the rotation dw_1/dx of the cross-section, gives

$$\frac{dw}{dx} - \frac{dw_1}{dx} = \gamma = \frac{Q}{G_c A_1}, \quad A_1 = (2c + f)b. \tag{7.29}$$

The axial strain in the face sheet at the mid-face location is $-(c + f/2)d^2w_1/dx^2$ (from bending theory). Therefore the resultant axial forces at the faces (compressive at the upper face and tensile at the lower) are

$$P_f = E_f(fb)\left(c + \frac{f}{2}\right)\frac{d^2w_1}{dx^2}. \tag{7.30a}$$

The bending moment can now be written as

$$M = P_f(2c + f) + 2M_f \quad \text{where} \quad M_f = E_f\frac{bf^3}{12}\frac{d^2w}{dx^2}. \tag{7.30b}$$

Using (7.30a) gives

$$M = E_f I_1\frac{d^2w_1}{dx^2} + E_f I_f\frac{d^2w}{dx^2} \quad \text{where} \quad I_1 = bf\frac{(2c + f)^2}{2}; \quad I_f = \frac{bf^3}{6}. \tag{7.31}$$

Now differentiating Equation (7.29), expressing from this d^2w_1/dx^2 and substituting it into Equation (7.31), gives

$$\frac{d^2w}{dx^2} = \frac{M}{(EI)_{\text{eq}}} + \frac{1}{G_c A_1(1 + I_f/I_1)}\frac{dQ}{dx}, \tag{7.32a}$$

where

$$(EI)_{\text{eq}} = E_f(I_1 + I_f), \tag{7.32b}$$

i.e., the equivalent bending rigidity is again due to the face sheets only but the bending rigidity of the faces about their own separate centroidal axes is included.

This equation essentially means that the total curvature d^2w/dx^2 is the sum of the flexural curvature and the curvature due to shear, i.e. the same basic approach as Engesser's, see Equation (7.3a), with

$$\frac{\beta}{AG_{\text{eq}}} = \frac{1}{G_c A_1(1 + I_f/I_1)}. \tag{7.33}$$

Proceeding in the same way as before, the critical load is obtained in the same form as Equation (7.8) with $\beta/(AG_{\text{eq}})$ defined in (7.33) and the Euler load P_E based on the bending rigidity (7.32b).

7.5 Huang and Kardomateas Shear Correction Formulas

A shear correction formula for sandwich columns in terms of the face sheet and core geometrical and mechanical properties was presented in Huang and Kardomateas (2002). This formula can be used in either the Engesser (7.8), or the Haringx (7.13) expression. It essentially provides for proper definitions of $(EI)_{\text{eq}}$, G_{eq} and β for the sandwich section.

In particular, the equivalent bending rigidity includes both the face sheets and the core and the bending rigidity of the faces about their own separate centroidal axes is included. Referring again to Figure 7.2, the equivalent flexural rigidity of the sandwich section is

$$(EI)_{\text{eq}} = 2E_f \frac{bf^3}{12} + 2E_f bf\left(\frac{f}{2}+c\right)^2 + E_c \frac{b(2c)^3}{12}. \tag{7.34}$$

Denoting the shear stresses in the face sheet and the core by $\tau_f(x,z)$ and $\tau_c(x,z)$, respectively, we can write the shear energy in the sandwich beam as

$$\begin{aligned} U_\gamma &= b\int\int \frac{\tau^2(x,z)}{2G(z)}dzdx \\ &= 2b\left\{\int_0^L\int_c^{c+f}\frac{\tau_f^2(x,z)}{2G_f}dzdx + b\int_0^L\int_0^c\frac{\tau_c^2(x,z)}{2G_c}dzdx\right\}. \end{aligned} \tag{7.35}$$

An "effective" or "equivalent" shear modulus for the sandwich section, G_{eq}, which includes the contribution of the face sheets, can be defined based on the compliances of the constituent layers, as follows:

$$\frac{2f+2c}{G_{\text{eq}}} = \frac{2f}{G_f} + \frac{2c}{G_c}, \tag{7.36}$$

where G_f is the shear modulus of the face sheets and G_c the shear modulus of the core. Equation (7.36) shows that when the core is of very low modulus, the second term would dominate and G_{eq} would approach G_c.

Now, assume that the shear stress is distributed in a uniform fashion over the entire section, $A = b(2c+2f)$, then the corresponding equivalent shear stress and strain are

$$\tau_{\text{eq}} = \frac{V(x)}{A}; \quad \gamma_{\text{eq}} = \frac{\beta V(x)}{G_{\text{eq}}A}, \tag{7.37}$$

where β is the shear correction coefficient, which takes into account the nonuniform distribution of shear stresses over the entire cross-section.

Then, the energy due to shear is

$$U_\gamma = A\int \frac{1}{2}\tau_{\text{eq}}\gamma_{\text{eq}}dx = \frac{\beta}{2G_{\text{eq}}A}\int_0^L V^2(x)dx, \tag{7.38}$$

Now the shear stresses, from simple bending theory, are distributed as follows:

- *Face sheets*

$$\tau_f(z) = \frac{V}{(EI)_{\text{eq}}}\frac{E_f}{2}\left[(f+c)^2 - z^2\right]. \tag{7.39a}$$

- *Core*:

$$\tau_c(z) = \frac{V}{(EI)_{\text{eq}}}\left[E_f f\left(\frac{f}{2}+c\right) + \frac{E_c}{2}\left(c^2 - z^2\right)\right]. \tag{7.39b}$$

Substituting into Equation (7.35) gives

$$U_\gamma = \frac{b}{(EI)_{\text{eq}}^2}\left(\frac{a_f}{G_f} + \frac{a_c}{G_c}\right)\int_0^L V^2 dx, \tag{7.40}$$

where

$$a_f = \frac{E_f^2}{4}\left[(f+c)^4 f - \frac{7}{15}(f+c)^5 - \frac{c^5}{5} + \frac{2}{3}(f+c)^2 c^3\right], \tag{7.41a}$$

$$a_c = E_f^2 f^2 c\left(\frac{f}{2}+c\right)^2 + \frac{2}{15}E_c^2 c^5 + \frac{2}{3}E_f E_c f\left(\frac{f}{2}+c\right)c^3. \tag{7.41b}$$

Comparing (7.38) and (7.40) gives the shear correction as

$$\frac{\beta}{AG_{\text{eq}}} = \frac{2b}{(EI)_{\text{eq}}^2}\left(\frac{a_f}{G_f} + \frac{a_c}{G_c}\right). \tag{7.42}$$

For a homogeneous section (this can be most easily seen by setting $c = 0$, $A = 2fb$), $\beta = 6/5$, which is a well-established shear correction factor for a rectangular homogeneous section.

Notice that this shear correction formula is not exclusively based on the shear modulus of the core, but includes the shear modulus of the faces and the extensional modulus of the core. Hence, it can account for sandwich constructions with stiffer cores and/or more compliant faces.

It should also be noted that a more general formula for the transverse shear correction coefficient β, which is applicable to a sandwich section with dissimilar faces can be found in Huang and Kardomateas (2002). This formula is also given in Chapter 12 in conjuction with the debond buckling problem.

The shear correction formula (7.42) can now be used by substituting this expression for β in either the Engesser critical load formula (7.8) or the Haringx one (7.13), where P_E is the Euler load based on the equivalent rigidity (7.34).

7.6 Comparison of the Global Buckling Formulas

Let us consider a sandwich column with unidirectional carbon/epoxy faces and hexagonal glass/phenolic honeycomb core. The orthotropic carbon/epoxy face moduli are (in GPa): $E_1^f = 181$, $E_2^f = E_3^f = 10.3$, $G_{23}^f = 5.96$, $G_{12}^f = G_{13}^f = 7.17$; and the face Poisson's ratios: $\nu_{12}^f = \nu_{13}^f = 0.277$, $\nu_{32}^f = 0.400$. The orthotropic honeycomb core moduli are (in GPa): $E_1^c = E_2^c = 0.032$, $E_3^c = 0.300$, $G_{23}^c = G_{13}^c = 0.048$, $G_{12}^c = 0.013$; and the core Poisson ratios are $\nu_{12}^c = \nu_{32}^c = \nu_{31}^c = 0.25$.

The total thickness is considered constant at $h = 2f + 2c = 30$ mm, the length over total thickness, $L/h = 30$, and we examine a range of face thicknesses defined by the ratio of face sheet thickness over total thickness, f/h, between 0.010 and 0.20. Figure 7.5 shows the critical load for a simply supported sandwich column, normalized with the Euler load (without transverse shear), P_{E0}. The different formulas from the literature are plotted. Notice also that we use G_{13}^c in place of G_c in these formulas, which were originally derived for isotropy.

Since it is possible that face wrinkling could dominate the failure of the column for very thin face sheets (see Chapter 9), Figure 7.5 also shows the critical wrinkling load calculated from Allen's wrinkling formula (8.63a). It is indeed noted that wrinkling would dominate for ratios f/h below 0.02.

From these results we can make the following observations:

(a) Allen's thin-face formula (7.15) and the Bazant and Cedolin (1991) formulas (7.8) and (7.33) produce similar results. In Figure 7.5, the curves from these two formulas can hardly be distinguished.
(b) Allen's thick-face formula (7.27) and the Engesser formula (7.8) with the Huang and Kardomateas shear correction (7.42) give predictions which are also practically identical and the corresponding curves can hardly be distinguished in Figure 7.5.
(c) The transverse shear effect is very large and results in a critical load being about only one third of the Euler load for face sheet thickness ratios, f/h, above 0.10.

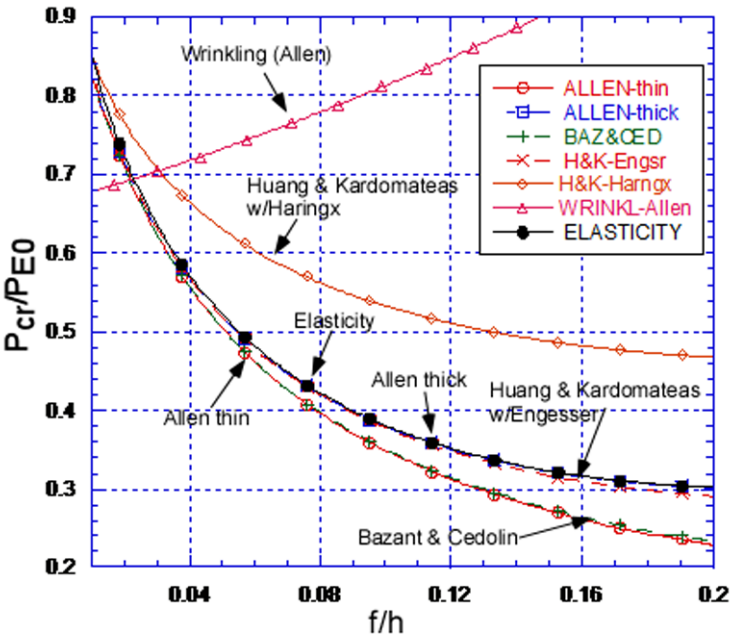

Figure 7.5 Critical loads for sandwich columns calculated from different formulas. The elasticity curve is from Kardomateas (2008b).

An exact three-dimensional elasticity solution to the problem was derived by Kardomateas (2008b). This solution can serve as a benchmark for assessing the accuracy of all these different formulas. From this solution, it was concluded that

(a) Allen's thin and thick-face formulas, the Bazant and Cedolin formula, and the Engesser formula with the Huang and Kardomateas shear correction are all conservative.
(b) Allen's thick-face formula and the Engesser formula with the Huang and Kardomateas shear correction are the most accurate, giving predictions almost identical to the elasticity value.
(c) Allen's thin-face formula and the Bazant and Cedolin formulas are accurate within about 5% of the elasticity value for f/h below 0.05, so they are very good for relatively thin face sheets; however, both give predictions that can be very conservative for the thicker face sheets (of the order of 20% below the elasticity value for $f/h = 0.2$).
(d) The Haringx formula gives predictions which are non-conservative and it is the most inaccurate, being of the order of 50% above the elasticity

value for $f/h = 0.2$. Its accuracy improves, though, for very thin face sheets.

One general observation is that the Haringx results stand out as being in much discrepancy with the elasticity results. This is in line with the discussion at the end of Section 7.2 and the statement that if a constant shear modulus G_c is used, then the correct theory is the Engesser-type theory and that the Haringx-type theory is usable only if the G_c of the core is considered to be a function of the axial stress in the face sheets (see also Bazant and Beghini, 2004).

Another general observation is that Allen's thick-face formula, Equation (7.27) and the Engesser formula, Equation (7.8) with the Huang and Kardomateas shear correction, Equation (7.42) are the most accurate, giving predictions almost identical to the elasticity value. The most popular formula, however, is Allen's thin-face formula, Equation (7.15), which is found to be very good for relatively thin face sheets but gives predictions that can be very conservative for the thicker face sheets.

Note regarding wide sandwich panels: In the foregoing formulas, when dealing with a wide panel, E_f must be replaced by $E_f/(1-\nu_f^2)$ where ν_f is the Poisson ratio of the faces, since in a wide panel, the lateral strains ε_{yy} must be zero, or else the bending could not be cylindrical and curvature would arise also in the lateral direction y. Therefore, with this modification, all of the previous formulas are also applicable to the buckling of wide sandwich panels.

7.7 First-Order Shear Deformation Analysis of Buckling of a Simply-Supported Sandwich Panel

Buckling of sandwich panels has been considered by several researchers and an excellent review of early work is presented in Plantema (1966). Solutions for plate buckling problems are also presented in the texts by Allen (1969) and Zenkert (1997). These solutions are derived using the approach of "partial deflections". In this section we will approach the buckling of a simply-supported sandwich panel using the classical first-order shear deformation approach outlined in Chapter 3.

A rectangular panel under biaxial compressive loading is considered, see Figure 7.6. The edges are loaded by uniform forces of magnitudes N_x and N_y. The initially flat symmetric sandwich plate is compressed until the flat shape deviates into a slightly bent mode shape once a critical set of loads

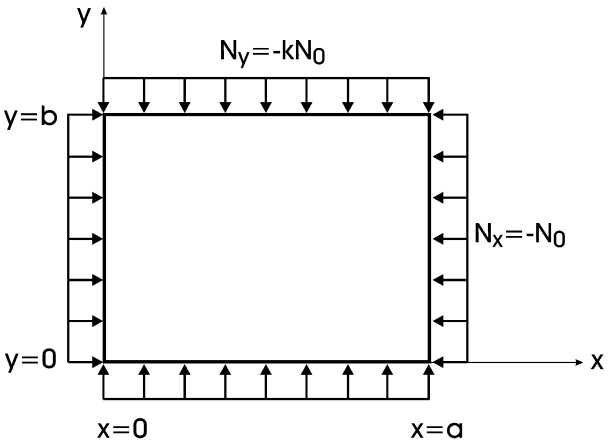

Figure 7.6 Sandwich panel under in-plane biaxial compressive loading.

(N_x and N_y) is reached. To determine the buckling loads and mode shapes the equilibrium equation (3.58e), which includes in-plane forces, is utilized with $q = 0$, and $N_{xy} = 0$,

$$\frac{\partial Q_x}{\partial x} + \frac{\partial Q_y}{\partial y} + N_x \frac{\partial^2 w}{\partial x^2} + N_y \frac{\partial^2 w}{\partial y^2} = 0. \tag{7.43}$$

Substitution of the expressions for the shear forces, Equations (3.68), yields

$$h_c G_{xz} \left(\frac{\partial \psi_x}{\partial x} + \frac{\partial^2 w}{\partial x^2} \right) + h_c G_{yz} \left(\frac{\partial \psi_y}{\partial y} + \frac{\partial^2 w}{\partial y^2} \right) + N_x \frac{\partial^2 w}{\partial x^2} + N_y \frac{\partial^2 w}{\partial y^2} = 0. \tag{7.44}$$

Simply-supported boundary conditions, see Section 3.2.3, are assumed

$$w(x, y) = M_x(x, y) = M_y(x, y) = 0. \tag{7.45}$$

These conditions apply along the edges $x = (0, a)$ and $y = (0, b)$ of the panel. The above boundary conditions are satisfied by

$$\psi_x = A_{mn} \cos \frac{m\pi x}{a} \sin \frac{n\pi y}{b}, \tag{7.46a}$$

$$\psi_y = B_{mn} \sin \frac{m\pi x}{a} \cos \frac{n\pi y}{b}, \tag{7.46b}$$

$$w = C_{mn} \sin \frac{m\pi x}{a} \cos \frac{n\pi y}{b}, \tag{7.46c}$$

where m and n are integers ($m = 1, 2, \ldots, n = 1, 2, \ldots$). Substitution of Equations (7.46) into (3.69c and d) and (7.44) yields the following matrix equation:

$$\begin{bmatrix} F_{11}F_{12}F_{13} \\ F_{12}F_{22}F_{23} \\ F_{13}F_{23}F_{33} \end{bmatrix} \begin{bmatrix} A_{mn} \\ B_{mn} \\ C_{mn} \end{bmatrix} = \begin{bmatrix} 0 \\ 0 \\ 0 \end{bmatrix}, \tag{7.47}$$

where

$$F_{11} = \frac{m^2\pi^2 D_{11}}{a^2} + \frac{n^2\pi^2 D_{66}}{b^2} + h_c G_{xz}, \tag{7.48a}$$

$$F_{12} = \frac{mn\pi^2(D_{12} + D_{66})}{ab}, \tag{7.48b}$$

$$F_{13} = \frac{m\pi h_c G_{xz}}{a}, \tag{7.48c}$$

$$F_{22} = \frac{n^2\pi^2 D_{22}}{b^2} + \frac{m^2\pi^2 D_{66}}{a^2} + h_c G_{yz}, \tag{7.48d}$$

$$F_{23} = \frac{n\pi h_c G_{yz}}{b}, \tag{7.48e}$$

$$F_{33} = \pi^2 \left[\frac{m^2 h_c G_{xz}}{a^2} + \frac{n^2 h_c G_{yz}}{b^2} + \frac{m^2 N_x}{a^2} + \frac{n^2 N_y}{b^2} \right], \tag{7.48f}$$

A non-trivial solution can be obtained by choosing N_x and N_y such that the determinant of the matrix $[F]$ in Equation (7.47) vanishes,

$$\det[F] = F_{11}(F_{22}F_{33} - F_{23}^2) - F_{12}(F_{12}F_{33} - F_{23}F_{13}) + F_{13}(F_{11}F_{23} - F_{22}F_{13}). \tag{7.49}$$

The only element of the matrix containing the in-plane loads N_x and N_y is F_{33} (Equation (7.48f)). With $\det[F] = 0$, Equation (7.49) gives the condition for a non-trivial solution in terms of F_{33}

$$F_{33} = \frac{F_{11}F_{23}^2 + F_{22}F_{13}^2 - 2F_{12}F_{13}F_{23}}{F_{11}F_{22} - F_{12}^2}. \tag{7.50}$$

In a typical problem, N_x and N_y are proportional,

$$N_x = -N_o, \tag{7.51a}$$

$$N_y = -kN_o, \tag{7.51b}$$

where N_o is the magnitude of compression load per unit length applied in the x direction. The critical buckling load is given by the set of m and n that minimizes the load N_o. The buckling mode is defined by the integers m and

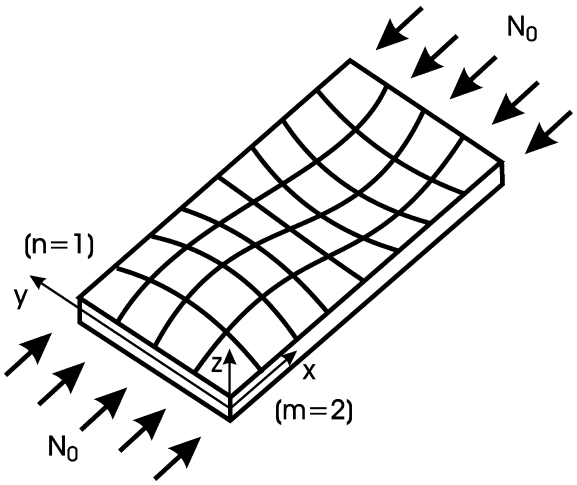

Figure 7.7 Illustration of buckling mode corresponding to $m = 2, n = 1$, where the panel buckles into a full sine wave in the x direction and a half sine wave in the y direction.

n defining the number of half sine waves into which the panel buckles in the x and y directions, respectively, see the expression for the panel deflection in Equation (7.48c) and the example $m = 2, n = 1$ shown in Figure 7.7.

We will specifically examine the buckling of a sandwich panel with isotropic core, $G_{xz} = G_{yz} = G_c$, under uniaxial compressive loading in the x direction, which in Equations (7.51) corresponds to $k = 0$. Equation (7.48f) applied to this loading yields

$$N_o = h_c \left(G_{xz} + \left(\frac{n}{m}\right)^2 \left(\frac{a}{b}\right)^2 G_{yz} \right) - \frac{a^2}{\pi^2 m^2} F_{33}, \tag{7.52}$$

with F_{33} given by Equation (7.50).

For numerical calculations, a square ($a = b = 0.5$ m) sandwich panel consisting of 2 mm thick unidirectional composite face sheets with the fibers aligned with the x axis (loading direction), and a 16 mm thick H100 PVC foam core was considered. The face and core mechanical properties are the same as those considered in Section 3.3. Calculation of the buckling load N_o for a set of values m and n was conducted based on Equation (7.52). Table 7.1 lists the results for $m = 1, 2, 3$ and $n = 1, 2, \ldots, 5$.

It is observed that the lowest buckling load (critical load) corresponds to a mode shape with one half sine wave in both the x and y directions $m = n = 1$. This is also the case for calculation of the critical load using classical laminated plate theory (CLPT) where transverse shear is not incorporated.

Table 7.1 Buckling load, N_o (in MN/m) for a square 0.5 m × 0.5 m sandwich panel with unidirectional composite face sheets and an isotropic H100 PVC foam core.

	$m=1$	$m=2$	$m=3$	$m=4$	$m=5$
$n=1$	0.7235	0.8856	0.9331	0.9500	0.9569
$n=2$	1.6013	1.1439	1.069	1.0393	1.9221
$n=3$	4.1431	1.8081	1.3805	1.2255	1.1487

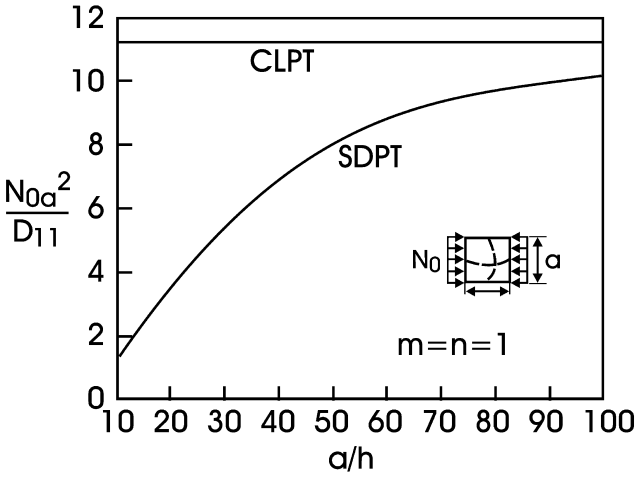

Figure 7.8 Critical buckling load for square sandwich panel vs. size calculated using shear deformation plate theory (SDPT) and classical laminated plate theory (CLPT).

For uniaxial compression of a square panel, CLPT yields (Whitney, 1987)

$$N_o = \frac{\pi^2}{a^2}\left(D_{11}m^2 + 2\left(D_{12}+2D_{66}\right)n^2 + D_{22}\frac{n^4}{m^2}\right). \tag{7.53}$$

The smallest buckling load for any panel occurs for $n = 1$. For the current panel with D_{11} much larger than D_{12}, $D_{22}$and D_{66}, the smallest value of N_o occurs for $m = 1$. This was found to be the case for any size of the square sandwich panel considered. Figure 7.8 shows the buckling load normalized with the bending stiffness D_{11}, and panel area a^2 plotted vs. the normalized side length.

It is observed that transverse shear deformation reduces the critical load. As the panel size increases, the difference between shear deformation plate theory and classical laminated plate theory decreases, similar to the bending case discussed in Section 3.3. For small panels, shear deformation has

a strong influence on the critical load and neglecting this important mode of deformation of sandwich panels will produce very unconservative estimates of buckling load. See also the results for sandwich columns presented in Sections 7.1–7.6.

7.8 Panel Compression Testing

It is general design practice of sandwich structures to determine the dimensions and supports of the panels to eliminate the possibility for buckling under service conditions. The experimental study of the buckling behavior of thin panels has been motivated by the emphasis of using structurally efficient materials in engineering applications such as naval ship structures, wind turbine blades, airplane structures, and packaging containers. In the analysis of such panels (see Section 3.2.3) idealized boundary conditions are imposed, typically "simply supported" or "clamped". These boundary conditions are introduced in order to obtain a tractable solution to the specific problem under investigation. In actual structures and experimental test fixtures, such idealized boundary conditions are often difficult to assess in a precise manner. Panel compression tests are commonly devised with the purpose of verifying an analytical or numerical finite element solution and to determine the actual mechanisms leading to the collapse of the panel such as localized buckling of the face sheets (face wrinkling) or compression failure of the face sheets. When performing testing for such purposes, it is important to assess the details on how the test fixture introduces load and how it supports the panel. In compression testing of sandwich panels into the post-buckling regime of the panel, the actual load-deformation behavior critically depends on the manner in which the edges of the panel are supported and how the load is introduced into the panel. Most experimental studies of the compressive response of thin panels have been focused on the implementation of simply supported boundary conditions, such as was discussed in the analysis of edge-loaded panels in Section 3.2.3. Simply-supported edge conditions are in this context commonly defined as being achieved by a fixture that allows all the edges to freely rotate around axes parallel to the edges and allows unconstrained movement of the edges in the plane of the panel, while restricting out-of-plane deflections. Farris and Filippov (1982), Khot and Bauld (1983), Souza et al. (1983), and Minguez (1986) have discussed several aspects of testing fixtures that provide support conditions close to the idealized boundary conditions.

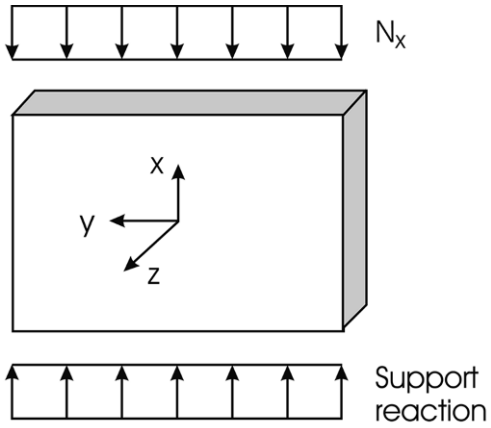

Figure 7.9 Schematic of uniaxial in-plane compressive loading of a sandwich panel.

Most experimental studies reported in the literature consider uniaxial compressive loading of panels. The testing of such panels is typically accomplished in a general-purpose vertical testing machine containing a metal fixture that allows the introduction of distributed load (line load) on the top horizontal edge while the vertical edges are unloaded, see Figure 7.9.

As the magnitude of the load is increased, the panel will deform in compression, and the upper horizontal edge will displace downwards. The vertical side supports in the test fixture must allow for such deformation. Furthermore, the edge supports should allow moment-free rotation of the edges of the panel.

Minguez (1986) designed a panel test where out-of-plane deflections of the vertical edges were constrained by attaching steel wires in regularly spaced slots machined along the edges, as shown in Figure 7.10. Each steel wire was attached to the panel using a brass collar with a set screw and a steel angle section fitting the machined slot. The ends of the wire were attached with screws to frames mounted on each side of the panel. The 80 cm long and 40 cm wide panel was supposed to buckle into one full sine wave along the loading direction and one half sine wave transverse to the loading direction. Minguez placed the wires 5 cm apart. To allow for sufficient tightening of the wires, high-strength piano wire was used.

A more common method to constrain out-of-plane deflection of the unloaded edges, is to use knife-edge supports (Figure 7.11). As will be discussed later, both the wire support and the knife-edge supports appear to approximate simply supported edge conditions, as judged from buckling mode

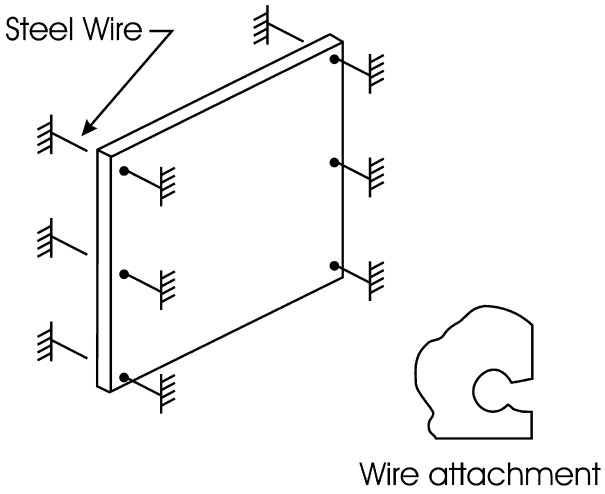

Figure 7.10 Edge support using regularly spaced steel wires.

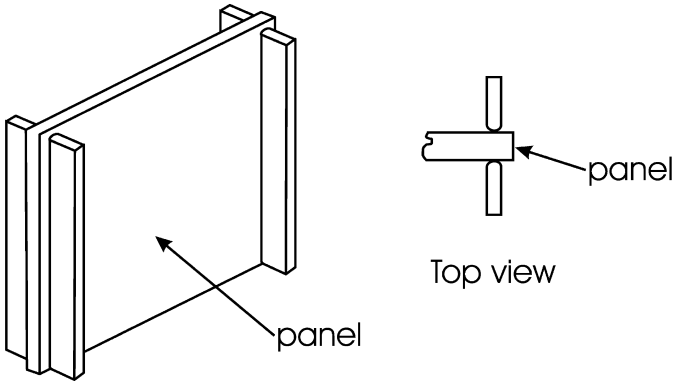

Figure 7.11 Knife-edge supports to constrain lateral deflections of the unloaded edges.

shapes and the magnitude of the measured buckling load. A disadvantage with the wire supports, however, is that the cut-outs for the steel wire attachments will weaken the panel. After buckling, the load distribution is no longer uniform and the compressive load becomes concentrated to the edge regions. If the panels are loaded to collapse, the cut-outs may reduce the ultimate load.

Minguez (1986) considered several other options for load introduction, see Figure 7.12. Each of the configurations shown in Figure 7.12 were employed for the directly loaded top and bottom edges. The flat plate configura-

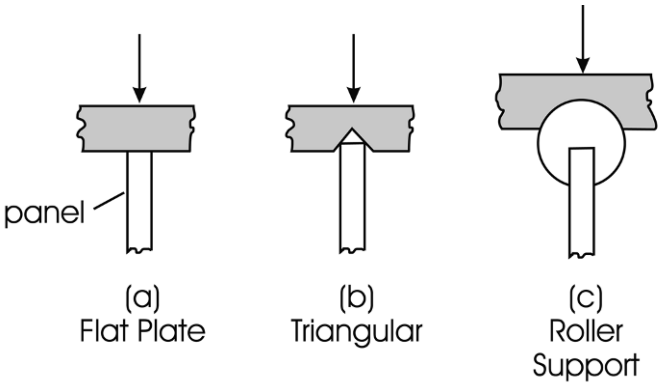

Figure 7.12 Methods for load introduction into sandwich panel.

tion, Figure 7.12a consisted of a flat stiff plate in direct contact with the panel edge. The triangular slot configuration, Figure 7.12b, used a loading platen with a triangular slot to maintain a straight edge during loading. For the roller support (Figure 7.12c) three configurations were used. The first consisted of two single rollers fitted to each loaded edge of the panel. The second roller configuration employed seven roller segments, each 5 cm long, fitted to the loaded edges. The third roller configuration used 13 independent 2.5 cm long roller segments on each loaded edge. By increasing the number of independent rollers, the out-of-plane deflection of the panel associated with buckling would become less and less constrained. Notice that the maximum edge rotation is expected to occur at the center of the edge, while the rotation near the corners should be close to zero. Before testing, lubrication was applied to the roller surface in contact with the circular slots in the loading plates to reduce friction. Nordstrand (2003) used a similar slotted roller arrangement as Minguez (1986), Figure 7.13, although the segments were shorter, approximately 1.7 cm, and the rollers were resting on needle bearings. For a panel size of 40 $\times$ 40 (cm) 23 segments were used on each horizontal edge.

The compression test fixture designed by Nordstrand (2003), moreover, employed an aluminum frame consisting of U-shaped extruded beams to provide rigid support to the panel. Knife-edge supports (Figure 7.11), were used to constrain out-of-plane deflections of the unloaded vertical edges. The upper loading beam was connected to the moving cross-head of the testing machine using a pin connection so that the panel is loaded uniformly before buckling and symmetrically after buckling, in the post-buckling regime. To maintain a load path along the undeformed reference plane of the panel, the upper loading beam was guided by two pairs of roller bearings in contact

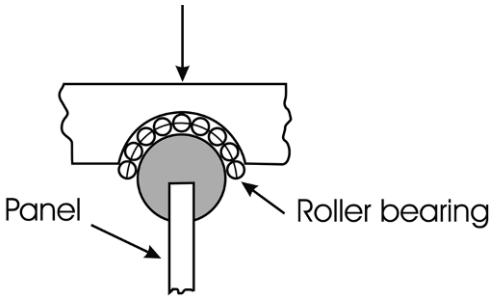

Figure 7.13 Rollers resting in circular lots supported by needle roller bearings.

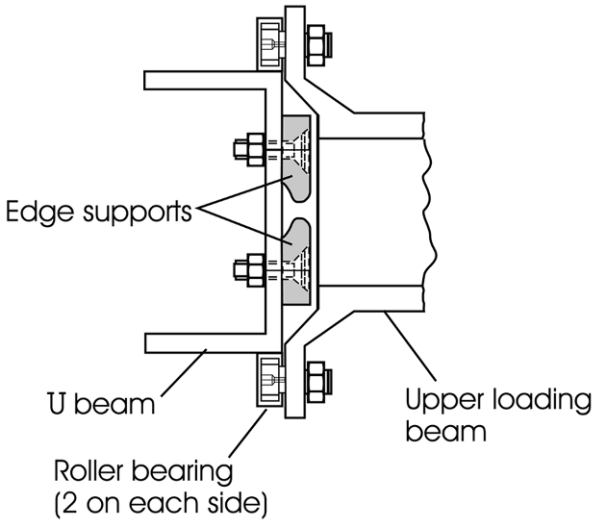

Figure 7.14 The upper loading beam is guided by two pairs of roller bearings in contact with the vertical U-beams of the compression test fixture.

with the outer surfaces of the vertical U-shaped beams, see the top view in Figure 7.14.

To examine whether a fixture is able to provide the desired loading and support conditions for a test panel, analytical and numerical predictions of the critical load and the associated buckling mode shape are compared to those determined experimentally. Such an approach seems very straightforward and it is for perfectly flat and defect-free panels. Actual panels, however, tend to deviate from the ideal flat form due to process-induced asymmetric residual stresses or other reasons. Hence, the panels tend to be slightly bent or warped in the unloaded state and when external loads are applied the

panel deforms further without any obvious indication of a bifurcation behavior.

Experimental studies have shown that the out-of-place deflection is much more indicative of buckling than the in-plane deformations. Consequently, several methods to monitor the out-of-plane deflection have been developed. The most simple methods determine the deflection at a point, such as the crest of a buckle, or several points, using deflectometers or non-contact laser interferometry. More sophisticated methods enable measurement of the full displacement field for the deflected panel. Such methods are the shadow-moiré method (Sciammarella, 1982), and the more recent digital image correlation technique described by Helm et al. (1996).

Once the load vs. out-of-plane deflection response has been measured, there are several methods available to determine the buckling load from the measured data. A commonly applied method is the Southwell graphical procedure outlined in Appendix C. This method was developed by Southwell (1932) for the evaluation of the buckling load for slightly bowed simply-supported columns. This method amounts to plotting the column deflection, w, vs. deflection divided by the load (w/P). The slope of the line represents P_{cr}, see e.g. the article by Souza et al. (1983). Such a method is adequate for structural members such as columns that display "neutral" post-buckling response (see Figure 7.15).

Neutral post-buckling response means that the load remains constant after buckling as long as the material is loaded within the elastic regime. A perfect column would buckle at a load, $P = P_{\text{cr}}$, which would remain constant up to very large deflections. Perfect here means that the column is initially straight and that the load acts along the specimen centroidal axis. Figure 7.15 shows the load, P, vs. additional out-of-plane deflections, w, for the perfect column. w_o represents the amplitude of the initial imperfection. Hence, the total out-of-plane deflection is $w_T = w + w_o$. w is the deflection one would measure after zeroing the displacement gage before load application. During compressive loading of an imperfect column, the column would already deflect at small applied loads and the load would asymptotically approach the buckling load at large deflections.

It can be readily observed that there are substantial difficulties in accurate determination of P_{cr} from experimental data for imperfect columns. The Southwell method (Appendix C) has proven to be an excellent method to determine the buckling load for columns. Panels loaded past the critical load, on the other hand, display a stable post-buckling response (see Figure 7.15), meaning that the panel can support loads substantially greater than the critical load. A perfect panel ($w_o = 0$) would not display any out-of-plane dis-

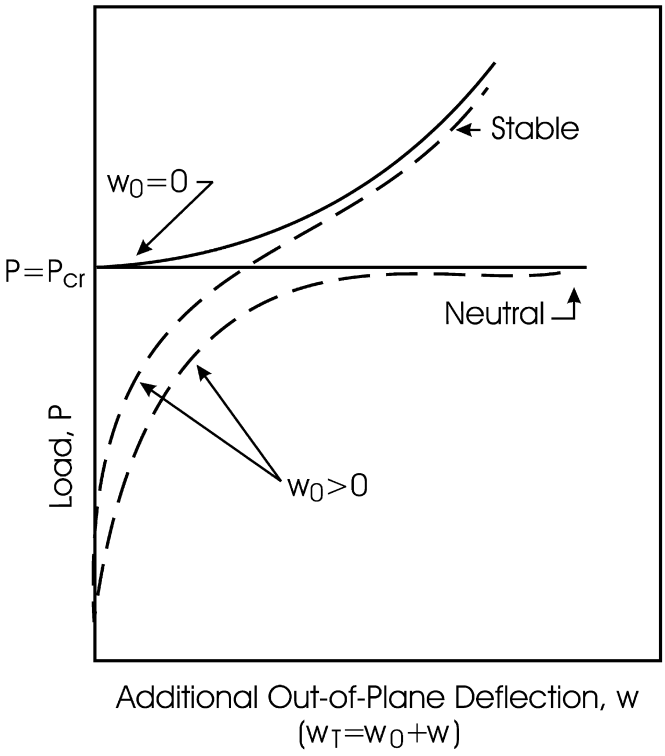

Figure 7.15 Illustration of neutral and stable post-buckling response.

placement until the critical load, P_{cr}, is reached. After such a panel buckles, the load will steadily increase until the material yields. Notice that a sandwich panel may fail by local buckling (wrinkling or intercell buckling, see Chapters 1 and 8).

As may be observed in Figure 7.15, extraction of the buckling load (P_{cr}) from the experimentally measured load vs. out-of-plane displacement record for an imperfect panel is not straightforward. Minguez (1986) applied the Southwell method to extract P_{cr} from the measured load vs. out-of-plane displacement (P–w) response of an aluminum panel under the various edge boundary conditions shown in Figure 7.12. In addition to the determination of P_{cr}, Minguez (1986) also examined the buckling mode shapes along and transverse to the panel. Figure 7.16 shows an example of mode shapes along and transverse to the loading direction for a panel loaded using the triangular slotted configurations shown in Figure 7.12b. The results show that all load introduction configurations produced a mode shape in agreement with

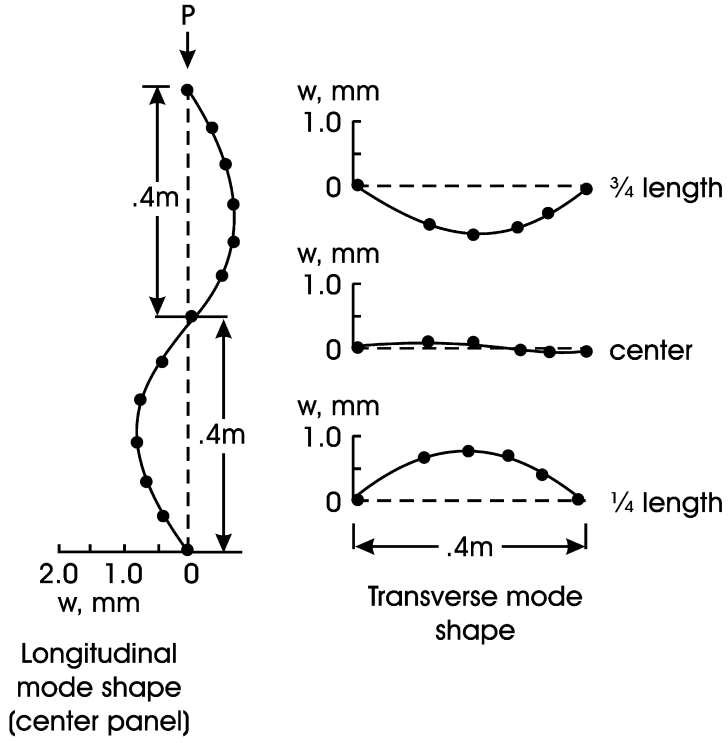

Figure 7.16 Buckling mode shape for a rectangular aluminum panel loaded using a triangular slot configuration. Data from Minguez (1986).

predictions (full sine wave along loading direction and half sine wave transversely).

Quantitatively, however, Minguez (1986) found that the various methods of load introduction produced substantially different amplitudes of deflection. It was found that the method of using 13 segmented rollers on each loaded edge (Figure 7.12c) produced the largest deflections at any given load above P_{cr}. This arrangement allows each section of the load-carrying edges to accommodate the buckling shape (Figure 7.16) with the maximum slope (rotation) at the center. Southwell plots were constructed for each load introduction configuration (Figure 7.12), see the example of a Southwell plot shown in Figure 7.17 for the triangular slotted configuration.

The buckling load, P_{cr}, determined from the slope of the fitted line in Figure 7.17, is $P_{cr} = 2.88$ kN. Table 7.2 summarizes buckling loads determined from Southwell plots for the various load introduction configurations. Table 7.2 also lists the buckling loads normalized by the theoretical critical

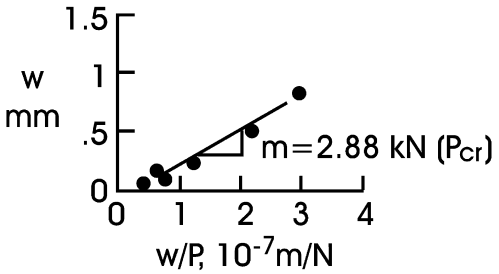

Figure 7.17 Southwell plot for panel with triangular slotted load introduction.

Table 7.2 Buckling loads for various load introduction configurations (Figure 7.7).

Load introduction	P_{cr} (exp), kN	$\frac{P_{cr}(exp)}{P_{cr}(SS)}$
Flat	N.A.	–
Triangular slots	2.88	1.11*
Rigid rollers	2.80	1.08*
13 roller segments	2.71	1.05*
Simply supported*	2.59	1.00*

* P_{cr}(SS) calculated from plate theory assuming simply supported (SS) boundary conditions.

load calculated for the panel assuming simply-supported edges (Minguez, 1986). For all load introduction configurations, the experimental buckling load exceeds the critical load by 5 to 11%, depending on the actual configuration. This result indicates that simply-supported conditions were not fully achieved for any of the configurations examined, although the one with 13 roller segments on each horizontal edge, provides boundary conditions close to simply-supported.

7.8.1 Experimental Determination of the Buckling Load of Panels

The method to extract the buckling load from the test results by Minguez (1986) was criticized by Chau (1987), because the Southwell method strictly applies only to columns, not to panels. To enable accurate experimental evaluation of the buckling load for panels, Spencer and Walker (1975) used load and deflection data in the pre- and post-buckling regimes of isotropic homogeneous panels in connection with a generalized Donnell (1938) equation,

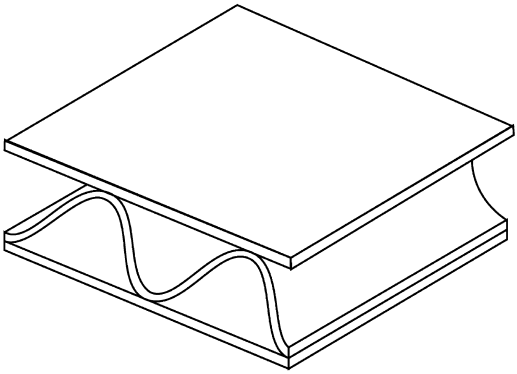

Figure 7.18 Element of a corrugated core panel.

$$\frac{P}{P_{\text{cr}}} = \frac{1}{w + w_o} + \frac{w + 2w_o}{(Ah)^2}, \tag{7.54}$$

where w_o and w are the initial out-of-plane imperfection, and w is the additional deflection. A is constant and h is the panel thickness. Equation (7.54) was fitted to the experimentally measured load (P) vs. out-of-plane displacement (w) data with w_o, A and P_{cr} as undetermined parameters to extract P_{cr}.

Nordstrand (2003) analyzed and tested orthotropic sandwich panels in uniaxial compression, as shown schematically in Figure 7.9. Geometric nonlinear analysis using classical plate theory without transverse shear deformation was developed by extending the post-buckling analysis of Rhodes and Harvey (1977) to an orthotropic panels with initial imperfection. This analysis yields an equation for the load (P) as a function of the out-of-plane displacement w, which contains the critical load as a parameter,

$$P = P_{\text{cr}}\left(1 - \frac{w_o}{w}\right) + \psi(w^2 - w_o^2), \tag{7.55}$$

where ψ is a post-buckling parameter. Consequently, this formula can be employed for experimental evaluation of the buckling load from measured load and out-of-plane deflection data.

Compression testing was done on 4 mm thick, 0.4 × 0.4 (m) corrugated core sandwich panels with an areal weight of 556 g/m^2. The corrugation wave length was 7.26 mm. Figure 7.18 shows the structure of corrugated core sandwich, a very common sandwich for packaging applications. Table 7.3 lists bending and shear stiffnesses of the sandwich panels.

Only reasonably flat panels with an imperfection of less than 2 mm (half thickness) were tested. The compression testing utilized a fixture described

Table 7.3 Bending and shear stiffnesses of corrugated core sandwich panels. h_c = core thickness = 3.51 mm.

Stiffness*	Value
D_{11}, Nm	14.6
D_{12}, Nm	2.71
D_{22}, Nm	5.43
D_{66}, Nm	3.34
$h_c G_{yz}$, kN/m	39.2
$h_c G_{xz}$, kN/m	5.6

*The in-plane principal directions refer to a coordinate system with the 1 axis perpendicular and the 2 axis parallel to the corrugations.

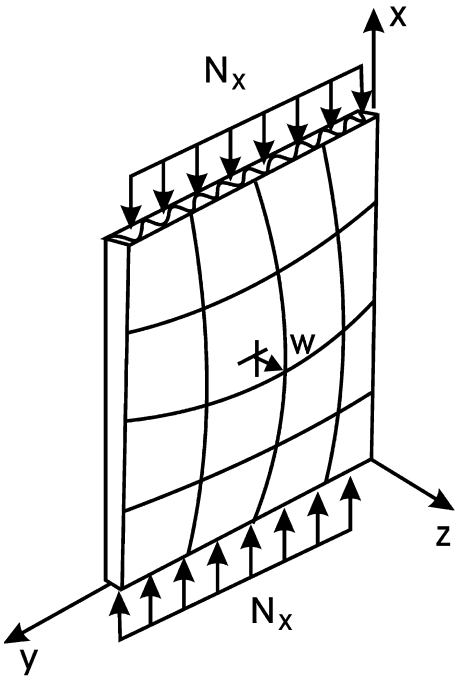

Figure 7.19 Uniaxial compression loading of corrugated core sandwich panel.

in connection with Figures 7.13 and 7.14. The panels were loaded uniaxially along the corrugations, i.e., the material direction "2" was along the loading axis as shown in Figure 7.19.

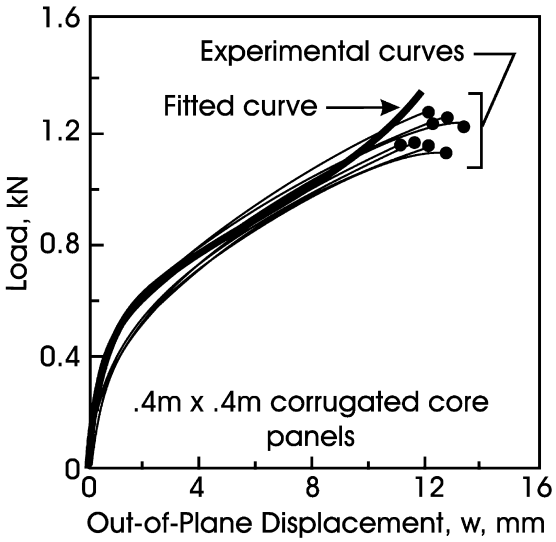

Figure 7.20 Experimental load vs. out-of-plane deflection curves for corrugated core sandwich loaded in uniaxial compression.

The out-of-plane deflection, w, was measured with a displacement gage at the panel center, where w should attain its maximum for buckling of the panel in its fundamental mode (Figure 7.19). The panels were loaded in displacement control until total collapse, as indicated by the circle at the end of each experimental P–w curve in Figure 7.20.

It is noted that the set of panels tested displayed quite a consistent response. The bold curve represents a fit of Equation (7.56) to the average experimental P–w curve using a commercially available software; SAS (2003). The fitting parameters are: $P_{\text{cr}} = 814$ N, $w_o = 0.8$ mm and $\psi = 3.55$ MN/m^2. It should be pointed out that the post-buckling analysis underlying the derivation of Equation (7.56) is a geometric nonlinear-elastic, and is not able to accommodate softening behavior due to the plasticity of the constituent materials. It is therefore essential that buckling occurs within the elastic regime of the material prior to localized buckling or yield.

It should be pointed out that the loading shown in Figure 7.18 refers to a panel loaded parallel to the corrugations and that the bending stiffnesses listed in Table 7.3 refer to a principal coordinate system (1-2) with the 1 axis perpendicular and the 2 axis parallel to the corrugations. To accommodate the loading configuration shown in Figure 7.19 the stiffnesses were transformed (Table 7.4). The first-order shear analysis presented in Section 7.7 was used to determine the critical buckling load for the sandwich panel with

Table 7.4 Transformed bending and shear stiffness for corrugated core sandwich panel (Figure 7.19).

Stiffness	Value
D_{11}, Nm	5.43
D_{12}, Nm	2.71
D_{22}, Nm	14.6
D_{66}, Nm	3.34
$h_c G_{yz}$, kN/m	5.6
$h_c G_{xz}$, kN/m	39.2

the data listed in Table 7.4. Calculations revealed that the panel should buckle in the fundamental mode ($m = n = 1$) at a load, $P_{\text{cr}} = 820$ N, which agrees very favorable with the critical load determined using the nonlinear regression analysis above, $P_{\text{cr}} = 814$ N.

7.8.2 Analysis of Collapse Load

As indicated in Figure 7.15, a distinctive feature of nearly flat slender sandwich panels is their ability to support loads significantly larger than the buckling load. Thus, in several situations the load design allowable load of such panels is governed by the collapse load rather than just the critical load. For the specific corrugated sandwich panel discussed earlier, the results in Figure 7.20, indicate that the collapse load exceeds the buckling load (814 N) by almost 50%.

The analysis of the collapse of sandwich panels is complicated by the fact that the strain in the middle plane of the panel due to buckling cannot be neglected once the panel is loaded above the buckling load. When the deflection, w, becomes comparable to the panel thickness, second-order terms in the expression for the components of strain in the middle plane of the plate must be taken into account, which substantially complicates the analysis of the buckling response (Timoshenko, 1936). As shown in Figure 7.15, the response of the panel is highly nonlinear and it becomes a formidable task to determine the distribution of load in the post-buckled panel. Such analysis shows that N_x becomes non-uniform and most of the load is supported by the regions of the panel near the unloaded edges, see Figure 7.21.

Because of the difficulties in analyzing the distribution of load in post-buckled panels, semi-empirical and simplified analytical approaches have

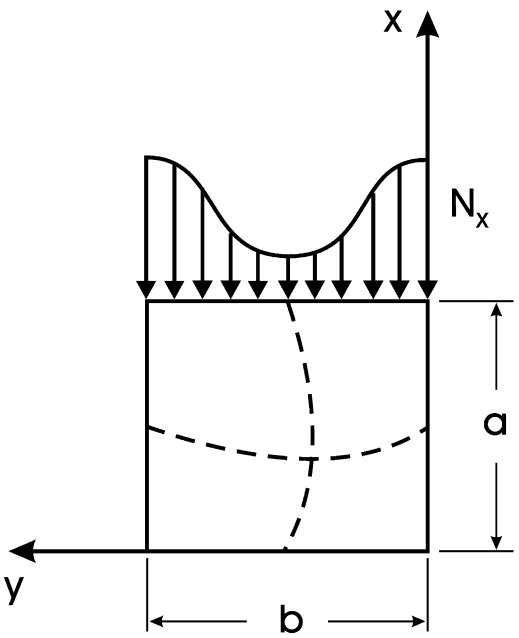

Figure 7.21 Distribution of compressive load in a panel loaded in uniaxial compression beyond the critical buckling load.

been developed. One of the early approaches to determining the post-buckling strength is attributed to Cox (1933), which was later modified by Norris (1942) for use with orthotropic materials such as plywood, and further modified for corrugated core sandwich panels by McKee et al. (1963). According to this approach, the compressive strength of the panel is assumed to follow a power function given by

$$\frac{P_{\text{col}}}{P_{\text{cr}}} = c\left(\frac{X_c}{P_{\text{cr}}}\right)^b, \tag{7.56}$$

where c and b are empirical constants, X_c is the uniaxial compressive strength of the sandwich in the direction of loading, and P_{cr} is the critical buckling load of the panel per unit width. To establish the parameter values for a given sandwich (X_c = constant), the size of the panel may be varied which results in variations of P_{col} and P_{cr}. To establish their numerical values, a logarithmic form of Equation (7.56) is used:

$$\log\left(P_{\text{col}}/P_{\text{cr}}\right) = \log c + b\log(X_c/P_{\text{cr}}). \tag{7.57}$$

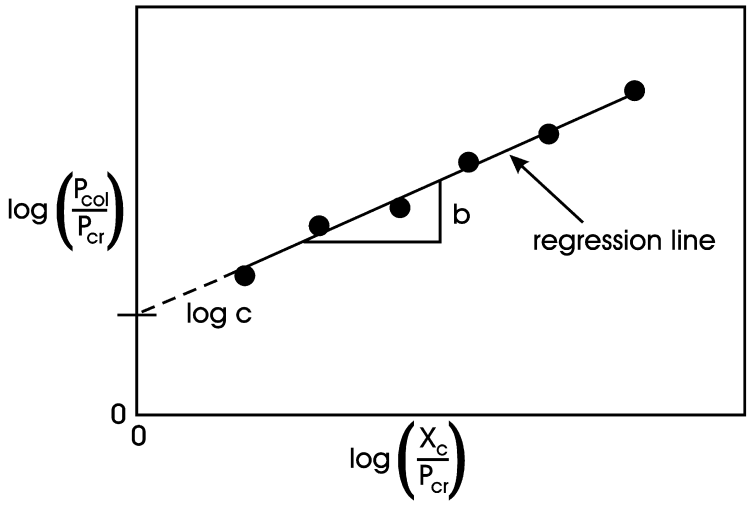

Figure 7.22 Determination of parameters c and b in the McKee et al. equation.

The critical buckling load is determined from analytical methods (see Section 7.7) or extracted from the experimental load vs. out-of-plane deflection curve, such as the one shown in Figure 7.20, using the methods described earlier in this section. The collapse load is also readily obtained from the experimental P–w curve. Once the data set has been established, a log-log graph may be constructed (Figure 7.22).

It is observed in Figure 7.22 that the slope of the linear regression line is b and the intercept with the vertical axis is log c. This method for strength determination has gained much acceptance within the corrugated board industry. Properly calibrated, the McKee et al. (1963) method produces reliable predictions of the collapse load of corrugated core packages. One shortcoming, however, is that the semi-empirical foundation requires experimental testing of several panels before new predictions can be made, and even if empirical data exits, there is always uncertainty about the accuracy of the predictions of sandwich panels that are different from those employed in calibration.

An approximate closed-form approach to predict the collapse load of panels loaded in uniaxial compression by a rigid frame into the post-buckling regime has been proposed by Timoshenko (1936). His analysis should also be applicable to relatively slender sandwich panels able to support loads greater than the critical buckling load. Since the panels are slender, it is here assumed that transverse shear deformation can be neglected. The critical

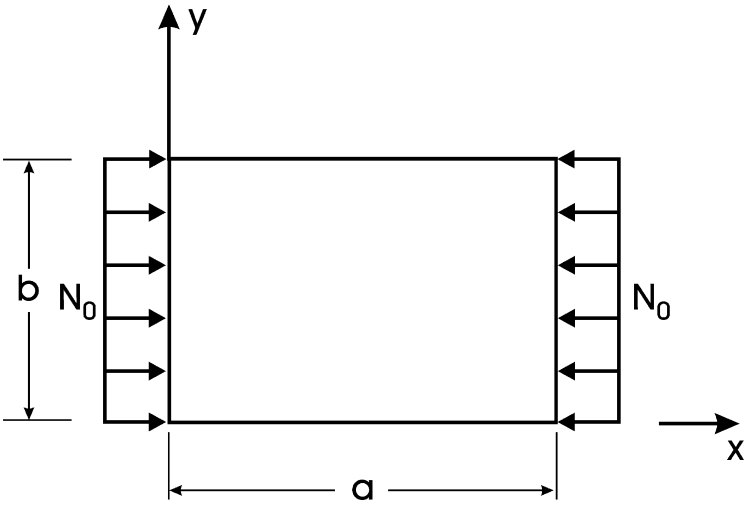

Figure 7.23 Uniaxial compressive loading of simply supported sandwich panel.

load, N_o of such a simply-supported panel loaded in uniaxial compression (Figure 7.23) is given by (Jones, 1999)

$$\frac{N_o b^2}{\pi^2 D_{11}} = m^2\left(\frac{b}{a}\right)^2 + \frac{2\left(D_{12}+2D_{66}\right)}{D_{11}} + \frac{D_{22}}{D_{11}}\left(\frac{a}{b}\right)^2\frac{1}{m^2}, \tag{7.58}$$

where m is the number of half sine waves into which the panel buckles in the direction of loading, i.e. the x direction. Recall that the panel buckles into one half sine wave transverse to the direction of loading. Analysis of sandwich panels under a more general loading configuration (see Section 7.7) shows that the number of buckling half-waves (n) in the y direction must in general be considered.

The number of half-waves the panel buckles into in the x direction, m, depends on ratios of the material stiffnesses and the panel aspect ratio (length/width ratio $= a/b$). Figure 7.24 shows the buckling load, N_o, normalized by the bending stiffness, D_{11}, and square of the width plotted vs. the panel aspect ratio for the following set of bending stiffness ratios $D_{22}/D_{11} = (D_{12}+2D_{66})/D_{11} = 0.1$.

It is observed that the buckling load corresponding to a particular mode shape (defined by the parameter m) undergoes a minimum at a certain panel aspect ratio and that the minimum gets more and more shallow as the aspect ratio increases. It is further noted that a square panel ($a = b$) would buckle into one half-wave ($m = 1$) while the minimum buckling load for long and

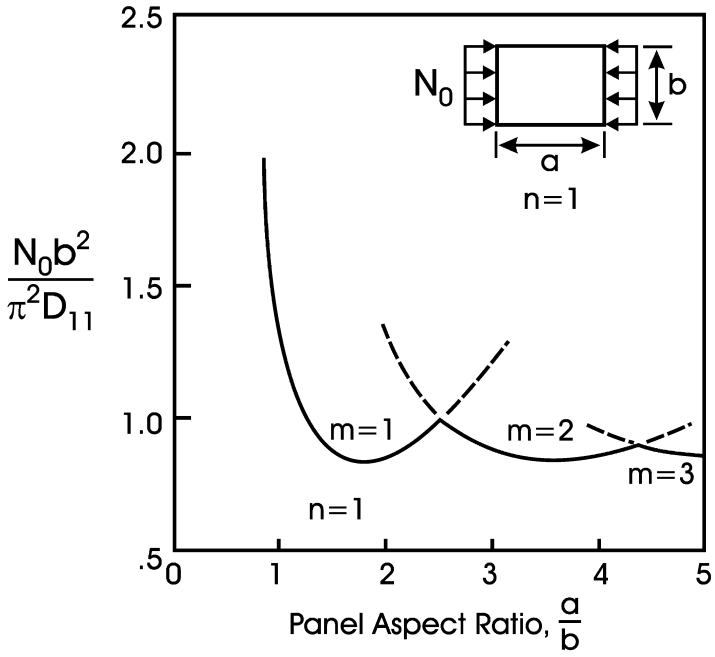

Figure 7.24 Buckling load of orthotropic panel loaded in uniaxial compression. $D_{22}/D_{11} = (D_{12} + 2D_{66})/D_{11} = 0.1$.

narrow panels (with a high aspect ratio, a/b) corresponds to $m > 1$, i.e., several half-waves.

Moreover, the minimum buckling load for each curve (with fixed value of m) does not depend on m. Detailed analysis based on Equation (7.58) reveals that each minimum occurs at an aspect ratio given by

$$a/b = m\sqrt[4]{\frac{D_{11}}{D_{22}}}. \tag{7.59}$$

The minimum buckling load, independent of the value of m is

$$\left(\frac{N_o b^2}{\pi^2 D_{11}}\right)_{\min} = 2\left[\sqrt{\frac{D_{22}}{D_{11}}} + \frac{D_{12} + 2D_{66}}{D_{11}}\right]. \tag{7.60}$$

Timoshenko (1936) presents an analysis of the post-buckling strength for a panel loaded in uniaxial compression based the distribution of load according to an approximation by von Kármán et al. (1932). As shown in Figure 7.21, most of the compressive after buckling is supported by the edge regions of

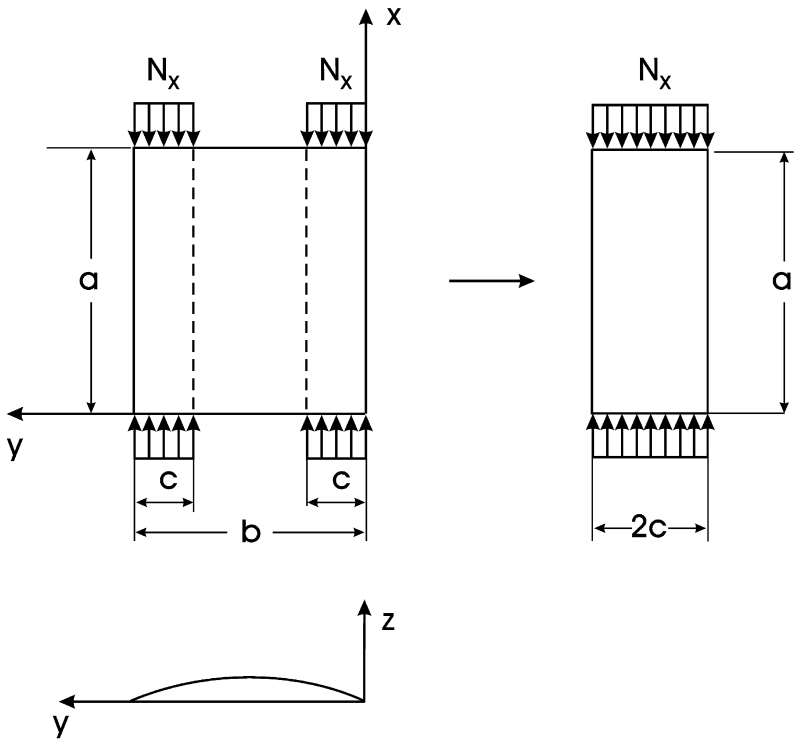

Figure 7.25 Timoshenko model of load distribution in post-buckled panel.

the panel. Timoshenko (1936) proposed that the load distribution in the post-buckling regime may be approximated by assuming a uniform load over each edge region of the panel, see Figure 7.25. The width of each such region is denoted by c. The middle region of the panel is completely disregarded, and the non-uniformly loaded panel of width, b, may be represented by a uniformly loaded panel of width, $2c$, Figure 7.25.

For a long narrow panel, the aspect ratio is much larger than 1, and such a panel is expected to buckle into several half-waves along the loading direction corresponding to a value of m greater than 1. The critical load for such a panel should approximately be equal to the minimum value, $(N_o)_{\min}$, as provided by Equation (7.60)

$$N_o = \frac{\pi^2}{2c^2}\left[\sqrt{D_{11}D_{22}} + D_{12} + 2D_{66}\right]. \tag{7.61}$$

Collapse of the panel is assumed to occur when the critical buckling load reaches the uniaxial compression failure load per unit width of the sandwich,

X_c. With this assumption ($N_o = X_c$) Equation (7.61) yields the width of the load-bearing region

$$c = \pi \left[\frac{\left(\sqrt{D_{11}D_{22}} + D_{12} + 2D_{66}\right)}{2X_c} \right]^{1/2}. \tag{7.62}$$

Hence, the collapse load of the panel is given by

$$P_c = 2cX_c = 2\pi \left[\frac{X_c}{2} \left(\sqrt{D_{11}D_{22}} + D_{12} + 2D_{66}\right) \right]^{1/2}. \tag{7.63}$$

Notice that the buckling factor within the parenthesis remains invariant if the directions 1 and 2 of the panel are interchanged. The only factor changing if the material directions 1 and 2 are interchanged is the compression strength, X_c.

Grangard and Rudstrom (1970) followed the Timoshenko analysis and derived an equation similar to (7.63) for the prediction of the collapse load of paperboard packages, but omitted the D_{12} stiffness which leads to under-prediction of the collapse load. To the knowledge of the authors, this analysis has not been applied to sandwich panels.

For the corrugated board panel examined by Nordstrand (2003), the bending stiffnesses D_{ij} are listed in Table 7.4. The uniaxial compression failure load per unit width of the sandwich, X_c is (Westerlind and Carlsson, 1992)

$$X_c = X_1 + X_2 + \alpha X_w, \tag{7.64}$$

where X_1, X_2, and X_w are the compressive strengths failure load per unit width of the two faces (1 and 2), and web (w), and α is the "take-up factor", i.e. length of web per unit width of the sandwich. For the core considered, $\alpha = 1.43$ (Nordstrand, 2003). With the strengths and thicknesses of the faces and web provided by Nordstrand (2003), Equation (7.64) yields $X_c = 4.16$ kN/m. Substitution of the strength X_c and the stiffnesses D_{ij} (Table 7.4) in Equation (7.63) yields a collapse load $P_c = 1{,}226$ N. This value may be compared to the experimental average from Figure 7.20, $P_c = 1{,}200$ N. This good agreement seems to support the simplified analysis, although more general acceptance would demand a much larger experimental data base.

An alternative analysis, which does not involve the empirical calibration of the McKee et al. (1963) approach, or the simplifying assumptions in the Timoshenko (1936) model, is to perform geometric nonlinear analysis to determine the stress distribution in the most highly stressed face sheet, which

would be the face on the concave side of the post-buckled panel subject to stresses due to axial compression and bending. Nordstrand (2003) conducted geometric nonlinear finite element analysis to determine the state of stress in the face sheets and used this in combination with a widely used biaxial failure criterion for orthotropic materials, viz. the "Tsai–Wu criterion" (Tsai and Wu, 1971). This analysis provided a collapse load of 1,270 N, in good agreement with the measured average collapse load, Figure 7.20, $P_{\text{col}} = 1,200$ N. Based on this favorable agreement Nordstrand (2003) concluded that local buckling or wrinkling of the face were not failure mechanisms governing the collapse load. However, once the panel reached the collapse load it was observed to fail in a face wrinkling mode leading to the collapse of the web core and collapse of the panel.